CrossMark

CAMBRIDGE
UNIVERSITY PRESS

RESEARCH ARTICLE

Heat-induced changes in molecular biosignatures and the influence of Mars-relevant minerals

Bettina Haezeleer, Stefan Fox (iD) and Henry Strasdeit (iD)

Department of Bioinorganic Chemistry and Chemical Evolution, Institute of Chemistry, University of Hohenheim, 70599 Stuttgart, Germany
Author for correspondence: Henry Strasdeit, E-mail: henry.strasdeit@uni-hohenheim.de

Abstract

The search for signs of life is a major objective in the exploration of Mars. Of particular interest are chemical biosignatures such as biomolecules. However, molecular biosignatures are susceptible to extreme environmental conditions such as heat, ionising radiation and strong oxidants. Therefore, a knowledge of the stability of possible biosignature molecules under present and past conditions on Mars is important, as well as the nature of possible alteration products. In the light of the long volcanically active history of Mars, we have studied the thermal behaviour of selected biological compounds, namely, haemin (an iron porphyrin closely related to the haem prosthetic group), cytochrome *c* (a small protein) and lecithin (a mixture of phospholipids). Samples were exposed to temperatures up to 900°C under an inert atmosphere of nitrogen, either in neat form or in mineral matrices. The matrix materials used were sodium chloride, gypsum ($CaSO_4 \cdot 2H_2O$), Ca-montmorillonite (STx-1b), the Martian regolith simulant JSC Mars-1A and some mixtures thereof. Key results are: (1) The onset of significant decomposition for haemin, cytochrome *c* and lecithin occurs around 240°C. At slightly higher temperatures the disappearance of all characteristic infrared spectral bands indicates complete decomposition and loss of the primary biosignatures. (2) Haemin stoichiometrically releases CO_2 and HCl during the initial thermal decomposition phase, at the end of which the iron porphyrin core is still intact. High-temperature products of haemin include graphite, α-iron and cementite (Fe_3C). (3) Neat lecithin forms long-chain polyphosphates at 500°C, whereas lecithin–NaCl mixtures form diphosphate (pyrophosphate). As these anions are absent and rare, respectively, in minerals, they may potentially serve as secondary biosignatures. (4) Heating a mixture of NaCl and JSC Mars-1A at 800°C in the presence of lecithin produces the aluminosilicate mineral sodalite ($Na_8[AlSiO_4]_6Cl_2$), which however appears to be of limited use as a secondary biosignature.

Contents

Introduction

Earth and Mars probably resembled each other in the environmental conditions early in their history (Strasdeit, 2010). This makes it conceivable that life may have evolved on both planets. Although today the surface of Mars is a hostile place (McKay, 2010), the climate was warmer and wetter during the late Noachian and early Hesperian periods, as indicated by the mineral composition of the crust and the presence of certain geological structures (Carr, 2012; Ehlmann and Edwards, 2014). Later, gradual cooling and aridification of Mars, related to decreasing volcanic activity, drastically reduced the surface habitability (Jakosky and Phillips, 2001; Solomon *et al.*, 2005; Kite, 2019). Consequently, potential life either had to escape the harsh surface conditions, for example by migration into the subsurface, became dormant or went extinct (Schulze-Makuch *et al.*, 2008; Westall *et al.*, 2015).

The search for life on Mars means searching for biosignatures such as intact microorganisms, metabolites, cell residues, biomolecules and their degradation products, physical structures (e.g. microfossils) and biominerals (Westall and Cavalazzi, 2011). Thermal processes together with minerals in the surrounding soil or rock matrix may have transformed chemical biosignatures into various relatively stable organic and inorganic compounds. These compounds may give hints about the existence of present or former life. Eruption events were an important source of thermal energy on Mars. Indeed, Mars' early history up to the end of the Hesperian period was characterized by volcanic activity resulting in lava flows and basin-filling lava flood events (Greeley and Spudis, 1981; Xiao *et al.*, 2012). Martian volcanism, including lava flows, extended to geologically recent times (until a few tens of millions of years ago) (Hauber *et al.*, 2011; Voigt and Hamilton, 2018).

Thermal decomposition products of biomolecules may still be detectable in Martian soil and rocks, particularly in the subsurface. Therefore, the rover of the ESA/Roscosmos' ExoMars mission will carry a drill to collect soil samples from a maximum depth of 2 m and a suite of analytical instruments to investigate the samples (Vago *et al.*, 2017). A visible and near-infrared spectrometer (Ma_MISS) for *in situ* mineralogical characterization of the bore hole is integrated in the drill tool (De Sanctis *et al.*, 2017). The most interesting drill core samples will be investigated by MOMA (a gas chromatograph–mass spectrometer), MicrOmega (a visible near-infrared hyperspectral microscope) and RLS (a Raman laser spectrometer) to identify potential biosignatures (Bibring *et al.*, 2017; Goesmann *et al.*, 2017; Rull *et al.*, 2017). Similarly, the Perseverance rover of NASA's Mars 2020 mission is equipped with a set of instruments capable of detecting chemical biosignatures (Farley *et al.*, 2020).

Some classes of biomolecules are found in all known organisms. Examples are porphyrin-type compounds, proteins and phospholipids. For this work we chose haemin (also called chlorohaemin or α-chlorohaemin), cytochrome *c* and lecithin, which is a mixture of phospholipids, as representatives of these three classes of biomolecules. Haemin (Fig. 1(a)) is a natural oxidation product of the haem prosthetic group, to which it is closely related structurally (Umbreit, 2007). The identification of alteration products of haem proteins is relevant to such diverse fields as geochemistry (Callot and Ocampo, 2000), forensic science (see e.g. Doty *et al.*, 2017), archaeology (see e.g. Dinegar, 1982; Petrone *et al.*, 2018), paleontology (see e.g. Schweitzer *et al.*, 1997; Greenwalt *et al.*, 2013) and astrobiology (Suo *et al.*, 2007). Cytochrome *c* is an evolutionary ancient haem protein which occurs in all three domains of life and is typically involved in electron transfer reactions (Fitch, 1976; Bertini *et al.*, 2006). Phospholipids are basic components of biological membranes (Van Meer *et al.*, 2008).

In what follows we describe the thermal decomposition of haemin, cytochrome *c* and lecithin and the properties of the residues formed. As minerals are known to influence the thermal behaviour of biomolecules (see e.g. Dalai *et al.*, 2017; Fox *et al.*, 2019), we not only investigated the neat compounds, but also performed thermolysis in mineral matrices. The matrix materials used were sodium chloride (NaCl), gypsum ($CaSO_4 \cdot 2H_2O$), the clay mineral Ca-montmorillonite STx-1b and the Martian regolith simulant JSC Mars-1A. Chlorides (possibly halite, NaCl), gypsum and montmorillonite are present at the Martian surface (Ehlmann and Edwards, 2014). Clay minerals are alteration products of volcanic rocks and were detected in the oldest Martian terrains, including Oxia Planum, the landing site for the ExoMars rover (Mandon *et al.*, 2021). The clay mineral STx-1b is particularly well characterized (Castellini *et al.*,
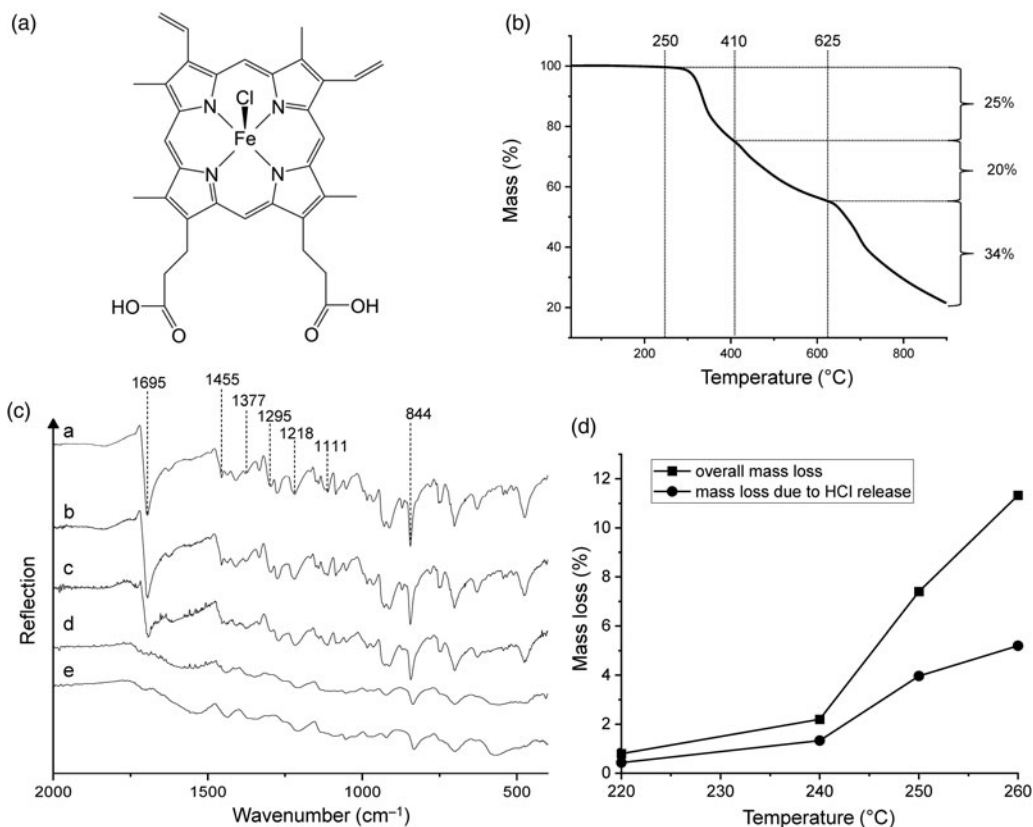
Figure 1. *(a) Chemical structure of haemin. (b) Thermogravimetric analysis of haemin under nitrogen gas at a heating rate of 5 K min^{-1}. (c) ATR infrared spectra of (a) haemin and of the products obtained from heating haemin at (b) 220°C, (c) 240°C, (d) 250°C and (e) 260°C. (d) Overall mass loss of haemin and mass loss due to HCl release after 48 h at different temperatures.*

2017). The regolith simulant JSC Mars-1A used in this study consists of altered volcanic ash (palagonite with relict plagioclase and clinopyroxene; Allen *et al*., 1998; Cloutis *et al*., 2015).

The aim of this work was to determine whether thermal alteration of biomolecules (including chemical interaction with minerals) forms organic and inorganic materials that can be useful as biosignatures. Such information may be helpful in interpreting data from current and future Mars missions.

Materials and methods

Chemicals and minerals

The following materials were used as received: haemin (Roth, ≥ 98%), cytochrome *c* (Sigma-Aldrich, ≥ 95%, oxidized form [ferricytochrome] with a reduced cytochrome *c* content ≤ 5%), soybean lecithin (Roth, ≥ 97% phospholipids), sodium chloride (VWR, analytical reagent), calcium sulphate dihydrate (gypsum, Sigma-Aldrich, Taufkirchen, Germany, ≥ 99%), STx-1b (The Clay Minerals Society, Chantilly, Virginia, USA) and JSC Mars-1A (Orbital Technologies Corporation [ORBITEC], Madison, Wisconsin, USA).

Pellet preparation

The biomolecules were used both as neat powders and as mixtures with the mineral matrices. The mixtures were studied as compact samples (pellets) which were prepared as follows. The organic and the

mineral component were dry-mixed and ground together in an agate mortar and pestle for ~2 min. The resulting average grain size was less than 10 μm, except for some haemin crystals which were up to 50 μm long. Then 200 mg of the resulting powder were pressed into a pellet using a hydraulic press. The pellets had a diameter of 13 mm and were ~1 mm thick. The mixtures with $CaSO_4 \cdot 2H_2O$, STx-1b or JSC Mars-1A contained 30% of the organic component. When NaCl was used, 10% of the organic component were usually sufficient because there was less analytical interference from the matrix material. An exception was the haemin–NaCl sample used for thermolysis at 800°C and subsequent X-ray powder diffraction (XRD) analysis, which was prepared with 30% of haemin.

Tube furnace experiments

The thermolysis apparatus used was essentially the one described by Fox and Strasdeit ([2013]). It consisted of a quartz tube positioned in a horizontal tube furnace. The tube was capped with two end pieces carrying the gas inlet and outlet. The open sample container was also made of thermally and chemically resistant quartz glass. After the container with the sample had been placed into the tube, the whole system was purged with nitrogen for at least 24 h to remove any oxygen. The sample was placed either (i) in the heating zone of the furnace before the temperature was raised or (ii) in the part of the tube outside the furnace and pushed into the heating zone when the furnace had reached its final temperature. In the first case the temperature was raised with a heating rate of $5\,\mathrm{K\,min^{-1}}$. The final temperature was between 150 and 900°C. Depending on the experiment, this temperature was held constant for 12 or 48 h. All experiments were performed under a slow stream of nitrogen. In some experiments, cold traps or gas washing bottles were inserted between the quartz tube and the gas outlet to collect volatile products.

Analytical instrumentation

Thermogravimetric (TG) analysis was performed with a TA Instruments TGA 550 in a nitrogen atmosphere ($\geq 99.999\%$, ≤ 3 vol ppm O_2 content). Samples of 1–8 mg were heated in platinum pans. The heating rate was $5\,\mathrm{K\,min^{-1}}$ and the temperature range was from room temperature to 900°C.

Transmission and ATR infrared spectra were obtained with a Nicolet 5700 FT-IR spectrometer (Thermo Fisher Scientific). For measurements in transmission mode, samples were embedded in NaCl (VWR, p.a.) or KBr (Roth, p.a.) pellets. The spectral range extended from 400 to $4000\,\mathrm{cm^{-1}}$, corresponding to 2.5–25 μm. Each spectrum was the average of 600 scans with a spectral resolution of $2\,\mathrm{cm^{-1}}$.

XRD data were collected on a Bruker D8 Focus diffractometer using $Cu_{K\alpha}$ radiation. Diffracted radiation was detected by a Sol-X energy dispersive detector except for the 800°C sample of haemin–NaCl (Fig. S2(c)), for which we used an SSD 160 detector (1D Si strip, nickel filter). Data were recorded in the 2Θ range 5–90° with a step size of 0.02° and counting times of 1 s per step (Sol-X) and 20 s per step (SSD 160). Reference diffractograms for haematite (RRUFF ID R040024), magnetite (RRUFF ID R060656), cementite (cohenite, RRUFF ID R100076) and sodalite (RRUFF ID R040141) were obtained from the RRUFF database (https://rruff.info/; Lafuente *et al.*, [2015]). Reference diffraction data for α-iron (database code 0011214) are available in the American Mineralogist Crystal Structure Database (http://rruff.geo.arizona.edu/AMS/; Downs and Hall-Wallace, [2003]).

Gas chromatography–mass spectrometry was performed with an Agilent 6890N/5973 GC/MSD system equipped with a DB-5MS column. Helium was used as carrier gas. Volatile products that were condensed in cold traps during thermolysis experiments were extracted with dichloromethane and then transferred to the GC-MS.

Chemical analyses

In order to quantify the evolution of HCl from haemin in moderate-temperature experiments (220–260°C), two gas washing bottles connected in series were inserted between the quartz tube and the gas outlet of the

thermolysis apparatus. The bottles were filled with a known amount of NaOH in aqueous solution. The gas flow was passed through the solutions by using fritted gas dispersion tubes. At the end of the thermolysis experiment, the amount of HCl absorbed was determined by the Mohr titration method: Chloride was precipitated as AgCl by titration with a $AgNO_3$ solution. K_2CrO_4 was used as indicator, and the end-point of the titration was reached when the formation of red-brown Ag_2CrO_4 started.

In order to quantify the loss of CO_2 from haemin at 260°C, two gas washing bottles filled with $Ba(OH)_2$ solution were inserted between the quartz tube and the gas outlet of the thermolysis apparatus. The CO_2 in the gas flow reacted with the $Ba(OH)_2$ to form solid $BaCO_3$. The amount of CO_2 released was then determined by back titration of excess $Ba(OH)_2$ with oxalic acid solution, with phenolphthalein as indicator. $Ba(OH)_2$ also reacted with the HCl evolved during the experiment, but we were able to take this into account because HCl was quantified independently (see above).

Elemental analyses were performed by Mikroanalytisches Labor Pascher, Remagen, Germany. The thermolysis residues of haemin had the following elemental compositions (in %): 260°C (means from two independent experiments): C 63.93, H 4.60, N 9.85, Cl 0.21, Fe 9.40, O (calculated by difference) 12.01; 500°C: C 70.56, H 1.61, N 11.1, Fe 11.5. These residues were hygroscopic. Therefore, the samples were dried at 60°C before analysis whereby the 260°C samples on average lost 5.5% of their mass. The total water content was ~12% (determined by drying at 150°C for 24 h). Thus, the 260°C samples used for elemental analysis contained ~6.5% (= 12 – 5.5%) water.

The residue from heating lecithin at 500°C was dried in vacuo at 60°C before analysis. Its elemental analysis gave the following results: C 50.57, H 1.62, N 2.11, P 14.5, O (calculated by difference) 31.2.

Results and discussion

Neat biomolecules

Haemin

Haemin is an iron(III) complex of protoporphyrin IX and chloride which contains iron in a square-pyramidal ClN_4 environment. Its structural formula is shown in Fig. 1(a). Iron porphyrins such as haemin are attractive biosignatures in the search for extraterrestrial life (Pleyer *et al*., 2022). In crystals of haemin the molecules are linked pairwise by hydrogen bonds between propionic acid side chains ($–CH_2CH_2COOH$) (Koenig, 1965; Kaduk *et al*., 2016). One of the carboxyl groups is in the vicinity of the chlorido ligand of a neighbouring molecule. Even though this is not a hydrogen-bonding interaction, it may play a role in the thermal decomposition pathway of solid haemin (see below).

TG analysis gave an initial picture of the overall thermal behaviour of haemin (Fig. 1(b); see Fig. S1 (a) for the first derivative curve). The decomposition onset temperature was determined to be ~250°C. The TG curve showed three major mass loss steps at 250–410, 410–625 and 625–900°C. The latter is caused by at least two thermal processes and was still incomplete at the end of the measurement. The corresponding mass losses were 25, 20 and 34%, and thus the total mass loss at 900°C was 79%. Wang *et al*. (2010) reported a smaller total mass loss under similar conditions (45% at 888°C), but the general TG curve shape was the same as in our experiments.

Figure 1(c) shows the infrared spectra of haemin and its 220, 240, 250 and 260°C thermolysis products. Diagnostic spectral features of untreated haemin include the strong C = O stretching band (1695 cm^{-1}), C–C (1455 cm^{-1}) and C–N stretching bands (1377 and 1111 cm^{-1}) and CH_2 and CH_3 deformation bands (1295, 1218 and 844 cm^{-1}; for band assignments see Dörr *et al*., 2008). After heating haemin at 240°C, the spectrum remained unchanged, demonstrating that the compound was essentially stable up to this temperature. However, when haemin was heated at 250°C, the bands were broadened, and most importantly, the C = O band was no longer present, indicating chemical transformation of the COOH groups. Concomitantly, a new, very broad band appeared at ~1560 cm^{-1}, which slightly shifted to ~1540 cm^{-1} in the spectrum of the 260°C residue. We tentatively assign this band to the asymmetric stretching mode of COO^- groups (see below).

The mass loss of haemin in constant temperature experiments at 220, 240, 250 and 260°C was 0.8, 2.2, 7.4 and 11.3%, respectively (Fig. 1(d)). Each experiment was conducted for 48 h. It should be kept in mind that the duration of the experiment is a key parameter that influences the mass loss at a given temperature. Our 48 h data indicate that the decomposition started slowly between 220 and 240°C, but it was too small to be detected by infrared spectroscopy. It should be noted that mass losses in constant temperature experiments occur at lower temperatures than in TG experiments (compare Fig. 1(b) and (d)). In other words, thermal processes appear delayed in TG curves, which is a well-known effect.

We identified two main processes that are involved in the initial decomposition of haemin, namely the protonation of the chlorido ligand (release of HCl) and the decarboxylation of one of the propionic acid side chains (release of CO_2 and formation of an ethyl group). If these processes were complete, they would result in a theoretical mass loss of 12.34% (5.59% from HCl and 6.75% from CO_2). This may be compared with the experimental value of 11.3% at 260°C, to which HCl contributed 5.2% (Fig. 1(d)) and CO_2 6.3%. Hence, the ratio between the experimental and the theoretical mass loss is 0.92. The 260°C samples used for elemental analysis had a water content of ~6.5% (see Materials and methods section). If we therefore assume (i) 92% complete decarboxylation of one of the two propionic acid groups, (ii) 92% complete reaction of the other propionic acid group according to equation (1) and (iii) a water content of 6.5%, then we calculate the following composition (experimental values in parentheses): C 64.28 (63.93), H 5.80 (4.60), N 9.06 (9.85), Cl 0.46 (0.21), Fe 9.04 (9.40), O 11.36 (12.01). It can be seen that there is reasonable agreement between the theoretical and experimental values.

HCl was formed by proton transfer from a carboxyl group to a chlorido ligand according to the following equation:

$$2\ FeCl\{PP(COOH)_2\} \longrightarrow FeCl\{PP(COOH)(COO)\} - Fe\{PP(COOH)_2\} + HCl \qquad (1)$$

$$(PP(COOH)_2 = \text{protoporphyrin IX dianion})$$

It is expected from chemical reasoning that the carboxylate group takes the place of the chlorido ligand and a Fe–OOC group is formed. The dimer in equation (1) only serves to illustrate the principle, and it is unknown whether it is an actual intermediate. Condensation products such as this one will react further by release of CO_2 and as proton donors to Cl^- until all carboxyl groups have been transformed. This explains the absence of the $C=O$ stretching band in the infrared spectra of the 250 and 260°C thermolysis products. The products were sparingly soluble in common organic solvents, indicating a polymeric structure. Their idealized formula is $Fe\{PP(H)(COO)\}$ where H stands for the ethyl group formed by decarboxylation. The presence of carboxylate groups is supported by a band at ~1540 cm^{-1} in the infrared spectrum which can be assigned to the COO^- asymmetric stretching mode (Deacon and Phillips, 1980). There are also candidates for the symmetric stretching band, but the assignment is ambiguous. Reaction 1 is probably facilitated by the relatively short distance of 4.11 Å between the chlorido ligand and a carboxyl O atom of an adjacent molecule in haemin crystals (Koenig, 1965).

The compound β-haematin (haematin anhydride, haemozoin, malaria pigment) is worth mentioning here. It consists of cyclic $[Fe\{PP(COOH)(COO)\}]_2$ dimers in which the monomers are connected by two Fe–OOC bonds (see e.g. Bohle *et al.*, 2012; Straasø *et al.*, 2014). β-Haematin can be prepared by HCl abstraction from haemin in solution, a process analogous to reaction 1. Note that in β-haematin half of the carboxyl groups are still intact, in contrast to our thermolysis products.

The iron porphyrin core was still present after treatment at 260°C, but this potential biosignature was progressively lost with increasing temperature. In 500 and 900°C experiments, the formation of carbonaceous material (amorphous carbon, graphite), iron oxides (magnetite Fe_3O_4, haematite Fe_2O_3), cementite (Fe_3C) and elemental iron (α-Fe) was observed (Fig. 2). In these experiments, haemin was first heated at 500°C for 48 h. Then half of the sample was removed for X-ray diffraction analysis. The diffractograms revealed the presence of amorphous carbon and magnetite (see e.g. Mochidzuki
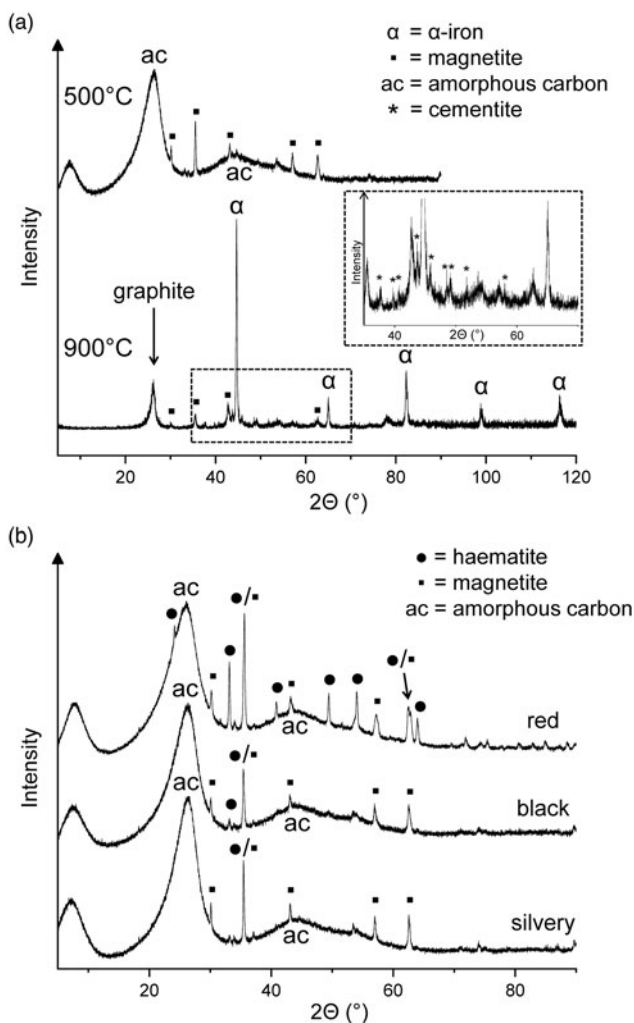
Figure 2. *(a) X-ray diffractograms of the residues obtained by heating haemin at 500°C for 48 h and at 900°C for another 48 h. (b) X-ray diffractograms of three differently coloured fractions of a residue obtained at 500°C from haemin.*

et al., 2003; Shi *et al.*, 2015). The other half of the sample was further heated at 900°C for another 48 h. The diffractogram of the 900°C residue was dominated by graphite and α-iron peaks with smaller peaks of magnetite and cementite (Fig. 2(a)). Obviously, the iron oxides and amorphous carbon which were present at 500°C reacted at higher temperatures to form metallic iron. This process is reminiscent of the reduction of FeO to Fe by carbon-bearing sediments in a basaltic melt (Klöck *et al.*, 1986).

One of the 500°C samples contained three differently coloured fractions (red, black and silvery), which could be manually separated. In addition to two prominent peaks of amorphous carbon, the X-ray diffractograms showed iron oxide peaks with haematite dominating in the red fraction and magnetite in the other two fractions (Fig. 2(b)). The iron oxides probably resulted from decomposition of the initially formed Fe–OOC groups (see above). Among the volatile products collected during the 500°C treatment of haemin, 2,3,4,5-tetramethylpyrrole and one of the isomers of ethyltrimethylpyrrole were identified by gas chromatography–mass spectrometry. However, the overall loss of volatile nitrogen compounds was small, judging from the N/Fe atom ratio of 3.85 in the solid residue, which was not significantly different from the value of 4.00 for haemin.

The question arises whether the high-temperature residues obtained from haemin at 500 and 900°C can be useful as biosignatures. Their formation is restricted to environments where the O_2 partial pressure is sufficiently low, as for example in the Martian atmosphere (Krasnopolsky, 2011). Otherwise burning would produce iron oxides as the only solid residues. The N/Fe atom ratio of ~ 4 present in the 500°C residue may be used as an indication that the product originated from an iron porphyrin, but in organisms iron porphyrins are embedded in proteins which would also contribute nitrogen. The close association of amorphous carbon with iron oxides and graphite with metallic iron is due to the special nature of haem as an iron-containing organic compound. However, it is unclear whether these specific constellations of products can serve as biosignatures. Additional methods such as stable isotope ratio measurements may provide further indications of possible biogenicity. But certainly the high-temperature residues are not 'strong' chemical biosignatures in the sense discussed by Fox and Strasdeit (2017).

Cytochrome c

Figure 3(a) shows the TG curve of cytochrome *c*. The corresponding first derivative curve can be found in Fig. S1(b). Evaporation of weakly bound water caused a mass loss of 3% during nitrogen purging at room temperature (hence the curve starts at 97%) and another 3% up to 130°C. This was followed by a major mass loss of 59% centred at 317°C and ending at ~470°C. The TG curve appears symmetrical in this temperature range. However, given that cytochrome *c* is a complex molecule and the mass loss is large, this step must consist of multiple chemical processes. Two further steps decreased the mass by an additional 30%, leading to a residual mass of 5% at 900°C. Anhydrous cytochrome *c* has an iron content of 0.45%. Therefore, the theoretical iron content of the 900°C residue was ~9%, under the reasonable assumption that no iron was lost on heating. Our TG results on cytochrome *c* essentially match those of Campos *et al.* (2004). Notable differences are that the literature curve is less structured and that the major mass loss step was observed at a higher temperature (~395°C compared to 317°C) with a larger mass loss (~76% compared to 59%). These deviations can be attributed to differences in experimental conditions, mainly to the considerably higher heating rate used in the literature study (20 K min^{-1}).

Infrared spectra of proteins show characteristic absorptions of the backbone amide groups. In the infrared spectrum of cytochrome *c* (Fig. 3(b)), such absorptions were found at 3275 and 3062 cm^{-1} (amide A and B band respectively, NH stretching), 1645 (amide I band, mainly C = O stretching), 1524 (amide II band, maximum at 1533 cm^{-1}, mainly NH bending and CN stretching) and 1240–1308 cm^{-1} (amide III region). The bands were assigned in accordance with the literature (Smith and Franzen, 2002; Barth, 2007). Absorptions at 2954, 2932 and 2869 cm^{-1} are caused by CH stretching vibrations. The 1394 cm^{-1} band is tentatively assigned to side chain vibrations; in particular, the symmetric COO$^-$ stretching modes of aspartate and glutamate residues are known to occur in this spectral region (Barth, 2007; Parikh *et al.*, 2011).

Exposure of cytochrome *c* to 150°C resulted in small but significant spectral changes (Fig. 3(b)). For example, the relative intensities of absorptions contributing to the amide II band changed (shifting the band maximum from 1533 to 1514 cm^{-1}) and the 1394 cm^{-1} band decreased in intensity and shifted to 1386 cm^{-1}. The infrared spectrum progressively changed with increasing temperature. While the 250°C spectrum is still recognizable as that of peptides or at least amides, the 300°C spectrum is completely different and shows none of the characteristic amide bands and also no CH stretching bands. Clearly the peptide structure was completely destroyed at temperatures between 250 and 300°C, and the residue was no longer an obvious biosignature. The 300°C spectrum is almost unstructured with broad bands around 3150, 1575 and 1230 cm^{-1} (Fig. 3(b)). It is reminiscent of the spectra observed for some carbonaceous materials with low H/C atomic ratios (see e.g. Russo *et al.*, 2014).

Lecithin

Soybean lecithin, which was used in this study, has been reported to contain the phosphodiester L-α-phosphatidylcholine (Fig. 4(a)) as a major component (Scholfield, 1981). In the TG curve of
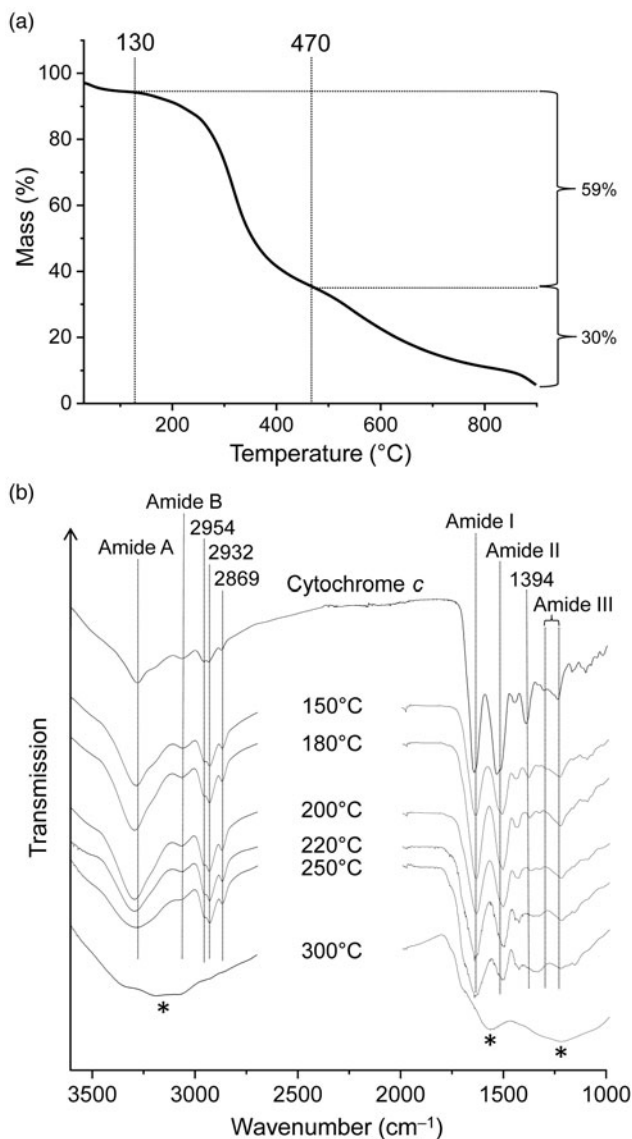
Figure 3. *(a) Thermogravimetric analysis of cytochrome* c *under nitrogen gas at a heating rate of 5 K min^{-1}. (b) Infrared spectra of cytochrome* c *and its thermal residues. New bands in the 300°C spectrum are marked by asterisks. The samples were measured in transmission mode in KBr pellets.*

lecithin (Fig. 4(b); see Fig. S1(c) for the first derivative curve), three mass loss steps were observed between 145 and ∼510°C, in good agreement with the results of Nirmala *et al.* (2011). The associated mass losses were 5, 70 and 8%. Slow mass loss continued beyond 510°C, and the total mass loss reached 88% at 900°C. The curve shape suggests that the second and largest decomposition step consists of different chemical processes, which is reasonable since lecithin is a mixture of many compounds. The temperature range of this step (190–385°C) encompasses the range in which characteristic infrared bands disappear and the utility of lecithin as a biosignature decreases strongly (see below).

The infrared spectrum of lecithin (Fig. 4(c)) showed a sharp, strong absorption at 1739 cm^{-1} due to the ester C = O stretching vibrations and three other prominent bands in the fingerprint region at 1467
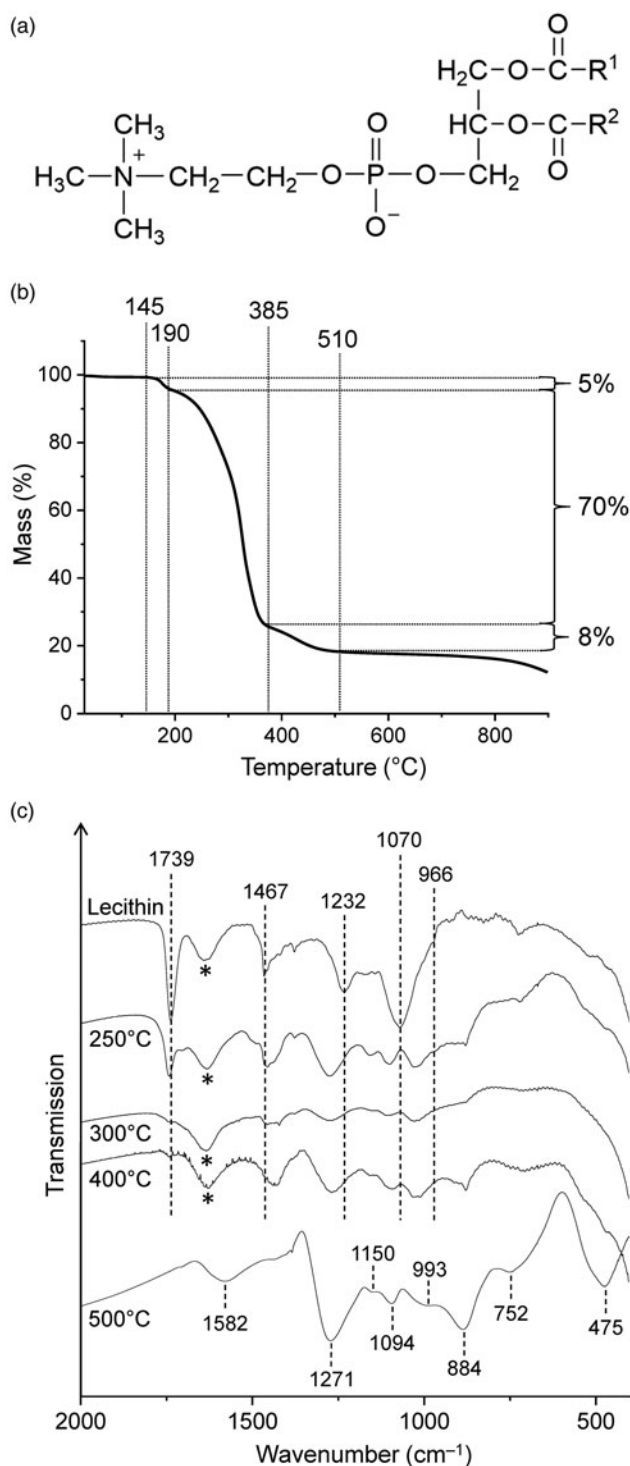
Figure 4. *(a) Chemical structure of L-α-phosphatidylcholine, a major component of lecithin (R^1, R^2 = fatty acid chain). (b) Thermogravimetric analysis of lecithin under nitrogen gas at a heating rate of 5 $K\,min^{-1}$. (c) Infrared spectra of lecithin and its thermal residues. The samples were measured in transmission mode in NaCl pellets except the 500°C residue which was measured in KBr. Asterisks mark the water bending band.*

(CH$_2$ scissoring), 1232 (asymmetric PO$_2^-$ stretching) and 1070 cm^{-1} (symmetric PO$_2^-$ stretching). The band assignments were made according to Tantipolphan *et al.* (2007) and Kudo and Nakashima (2020). The shoulder at 966 cm^{-1} was assigned to the asymmetric N–(CH$_3$)$_3$ stretching vibration of the choline group (Popova and Hincha, 2003). In addition, four bands at 3010, 2956, 2925 and 2853 cm^{-1} were observed in the CH stretching region (not shown in Fig. 4(c)).

After treatment at 250°C, most infrared absorptions of lecithin were still clearly evident, even though the maxima were shifted (Fig. 4(c)). The intensities also changed. For example, the C = O band was much weaker than in the spectrum of untreated lecithin, indicating that substantial decomposition occurred at 250°C. This finding is consistent with the TG data, which show that the onset temperature of the major mass loss step was 190°C (Fig. 4(b)). In contrast to the 250°C spectrum, lecithin was no longer recognizable in the spectrum of the 300°C residue. Thus in this respect lecithin behaved similarly to cytochrome *c* (see above).

New bands appearing at 1271, 1150, 1094, 993, 884, 752 and 475 cm^{-1} in the 500°C spectrum (Fig. 4(c)) strongly suggest the presence of linear long-chain polyphosphates (Corbridge and Lowe, 1954; Bues and Gehrke, 1957; Rao *et al.*, 2001). Such polyphosphates are known as thermal condensation products of dihydrogen phosphate (Greenwood and Earnshaw, 1997). They have the general formula (P$_n$O$_{3n+1}$)$^{(n+2)-}$ or approximately (PO$_3^-$)$_n$ for large values of *n*. The O/P atom ratio in the 500°C residue was 4.2 (see Materials and methods section) and thus more than sufficient for polyphosphates.

The presence of polyphosphates raises the question as to where the counter charge is located. We hypothesize that the carbonaceous matrix includes positively charged oxygen and nitrogen atoms, perhaps similar to those in pyrylium and quinolizinium cations, respectively (see e.g. Eicher *et al.*, 2012). A very weak broad CH stretching band is observed at 3035 cm^{-1} which is indicative of aromatic structures. There are no spectral features that can be attributed to specific cationic groups, but there is a conspicuous band at 1582 cm^{-1}, which lies in the region where hydrogen-poor carbonaceous materials have a characteristic absorption band (see e.g. Russo *et al.*, 2014). The spectra of these materials also show an extremely broad, weakly structured absorption extending from ∼1000 to ∼1450 cm^{-1}, which may be obscured by polyphosphate bands in the spectrum of the 500°C residue of lecithin. The black appearance and the high carbon (50.57%) and low hydrogen content (1.62%) of the residue are also consistent with the presence of carbonaceous material.

Interestingly, after heating lecithin at 900°C, no solid residue was observed but the quartz sample container showed clear signs of corrosion. Indeed, condensed phosphates ('metaphosphates') are known to attack quartz glass at high temperatures (Barz *et al.*, 1996).

Biomolecules in mineral matrices

On rocky planets such as Mars non-volatile organic materials will usually be in long-term contact with surrounding minerals. This prompted us to investigate the thermal behaviour of biomolecule–mineral mixtures. We limited our experiments to haemin and lecithin and the mineral matrices sodium chloride (NaCl, halite), Ca-montmorillonite STx-1b and Martian regolith simulant JSC Mars-1A. In the case of lecithin, also gypsum (CaSO$_4 \cdot$ 2H$_2$O) and a 1:1 mixture of NaCl and JSC Mars-1A were used as matrices. It is worth mentioning that gypsum loses most of its crystal water well below 200°C (Strydom *et al.*, 1995).

Figure S2 shows the X-ray diffractograms of residues obtained by heating haemin at 800°C in three different mineral matrices (STx-1b, JSC Mars-1A and NaCl). Graphite, α-iron and cementite were found in all cases. The diffractogram of the haemin–NaCl residue also contained magnetite peaks. Thus, the same products were observed as in the 900°C experiment with neat haemin (see above).

In some cases, the thermal treatment of lecithin in a mineral matrix gave products not observed from lecithin alone. In sodium chloride, for example, the phosphate esters decomposed to form the diphosphate anion (pyrophosphate, P$_2$O$_7^{4-}$), as is evident from the infrared spectra of the residues obtained between 400 and 700°C (Fig. 5(a)). The characteristic bands of diphosphate (Fig. S3; see e.g. Cornilsen and Condrate, 1978) are most clearly seen in the 500°C spectrum. If diphosphate was
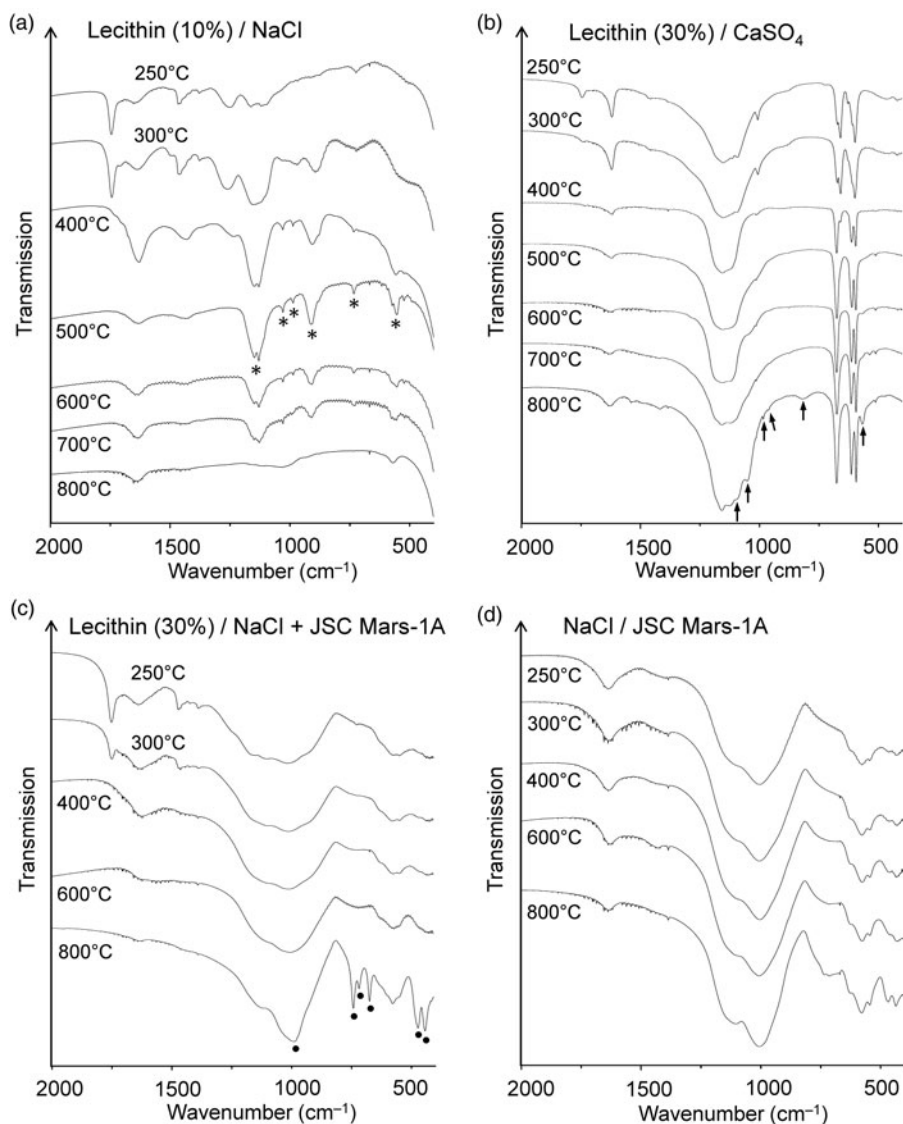
Figure 5. *Infrared spectra of the residues obtained from heating lecithin in (a) NaCl, (b) gypsum and (c) a 1:1 mixture of NaCl and JSC Mars-1A. Marked bands are assigned to diphosphate (*), phosphate-related anions (↑) and sodalite (●). (d) Spectra of the thermally treated mixture of NaCl and JSC Mars-1A for comparison. The samples were measured in transmission mode in NaCl pellets.*

also formed from neat lecithin, the amount was too small to be detected by infrared spectroscopy; indeed, it appeared that long-chain polyphosphates predominated (see above).

After heating lecithin–gypsum mixtures the lecithin C = O stretching band at ~1739 cm^{-1} was still visible at 250°C but had virtually disappeared at 300°C (Fig. 5(b)). This behaviour was very similar to that of neat lecithin (Fig. 4(c)). The infrared spectrum of the residue from the thermolysis of lecithin–gypsum at 800°C showed several new bands. At this temperature gypsum is completely dehydrated. Accordingly, some of the bands could be unambiguously assigned to anhydrous CaSO$_4$ (Makreski *et al.*, 2005). However, six weak to very weak bands at 566, 819, 963, 983, 1052 and 1095 cm^{-1} could not be attributed to CaSO$_4$ (Fig. 5(b)). They lie in the spectral regions where the characteristic infrared absorptions of phosphates (PO$_4^{3-}$) occur (Jastrzębski *et al.*, 2011; Salama *et al.*, 2014).

The Martian regolith simulant JSC Mars-1A and the clay mineral STx-1b appeared to have no significant influence on the thermal decomposition of lecithin. The diagnostic ester band in the infrared spectrum ($\sim$1739 cm^{-1}) disappeared above 300°C (JSC Mars-1A) and 250°C (STx-1b), respectively (Figs S4 and S5). Complete decomposition of the ester groups in this temperature range was also observed for neat lecithin and lecithin in NaCl and CaSO$_4$. The infrared spectra of the residues formed from lecithin–JSC Mars-1A and lecithin–STx-1b between 250 and 800°C showed no bands that could be attributed to phosphate-related anions. If such anions had formed, their bands were too weak or broad to be observed against the matrix background.

When a 1:1 mixture of NaCl and JSC Mars-1A was used as the matrix for lecithin, the infrared spectra of the 400 and 600°C residues were virtually identical to those obtained without lecithin (Fig. 5(c) and (d)). However, after heating the lecithin–NaCl–JSC Mars-1A mixture at 800°C, new bands appeared that could be assigned to the aluminosilicate sodalite (Na$_8$[AlSiO$_4$]$_6$Cl$_2$) (Fig. 5(c)). A reference spectrum of sodalite is shown in Fig. S6. Sodalite also occurs naturally as a mineral (Deer *et al*., 2013; Hudson Institute of Mineralogy, 2022a). Interestingly, in the absence of lecithin, no new bands were observed after heating to 800°C (Fig. 5(d)). These results were confirmed by X-ray diffraction (Fig. 6). In addition, neither lecithin–NaCl (Fig. 5(a)) nor lecithin–JSC Mars-1A (Fig. S4) produced sodalite at 800°C. Thus, all three components together are essential for sodalite formation.

Synthetic sodalite can be prepared, for example, by high-temperature solid-state synthesis from the clay mineral kaolinite (Al$_2$Si$_2$O$_5$(OH)$_4$), sodium chloride and sodium hydroxide (Bardez *et al*., 2008). In our reaction system, JSC Mars-1A provides the aluminosilicate, namely calcium-rich feldspar with the end-member formula CaAl$_2$Si$_2$O$_8$ (Allen *et al*., 1998), and thus assumes the role of kaolinite. We believe that the strongly basic products that form from lecithin at high temperatures take the place of sodium hydroxide. These products were also responsible for the corrosion of the quartz sample containers at 900°C (see above).

Summary and conclusions

In this study we investigated the effects of temperature on haemin, cytochrome *c* and lecithin as biosignatures. All experiments were performed under an inert atmosphere of nitrogen. Our main results are as follows:

(1) The characteristic infrared absorptions of the neat samples were still present after heating at 240–250°C. Thus, the biomolecules were recognisable as such up to this temperature. At higher temperatures the characteristic absorptions disappeared completely.

(2) Haemin showed well-defined decomposition behaviour between $\sim$240 and 260°C where two processes occurred, namely decarboxylation and formation of HCl. The iron porphyrin core, which may serve as an important biosignature (Pleyer *et al*., 2022), remained intact at 260°C. However, it decomposed at higher temperatures.

(3) Solid inorganic products occurred at temperatures of 500°C and above: (i) Haemin formed amorphous carbon and iron oxides at 500°C, and graphite, metallic iron and cementite (Fe$_3$C) at 900°C. It is not clear whether these product mixtures can be used as biosignatures. But it may be noted that biological material can contain more than trace amounts of iron. Dried human red blood cells, for example, are composed of 95–98% haemoglobin (Kaza *et al*., 2021), corresponding to an iron content of 0.33%. Moreover, loss of volatile products during thermal decomposition will increase the percentage of iron in the residues. (ii) Heating of lecithin at 500°C produced linear long-chain polyphosphates, as indicated by the infrared spectrum of the residue. These anions do not occur in minerals (Pasek, 2020). Therefore, the presence of linear polyphosphates with more than three phosphorus atoms may tentatively be interpreted as a biosignature.

(4) In most cases, minerals did not greatly affect the thermal behaviour of the organic molecules. However, there were two remarkable exceptions for lecithin: (i) Diphosphate (pyrophosphate) was observed as a thermolysis product in sodium chloride between 400 and 700°C. This differs
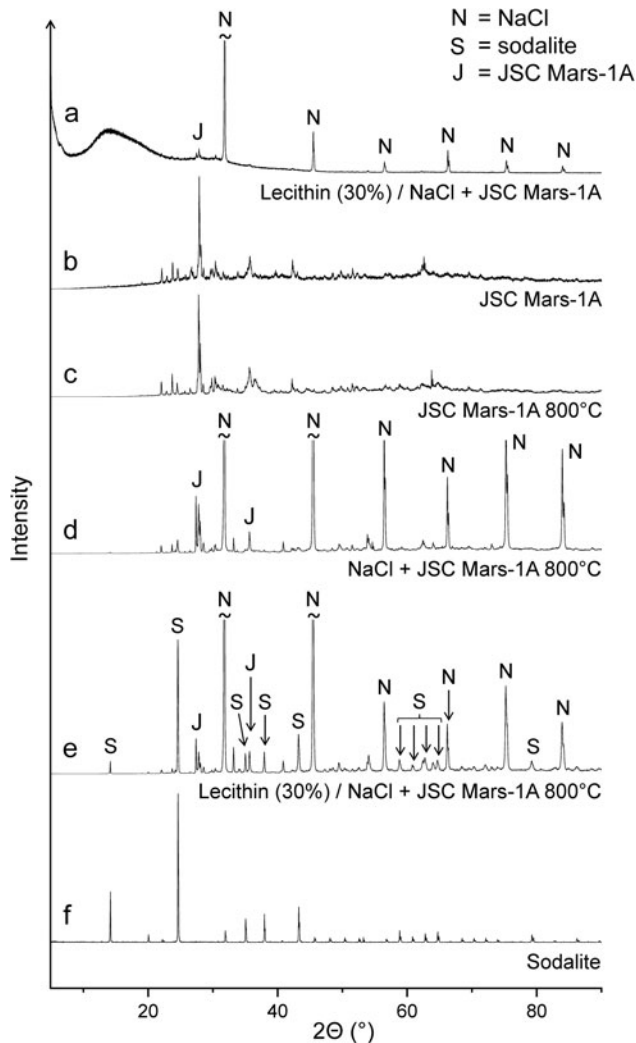
Figure 6. *X-ray diffractograms of (a) the lecithin–NaCl–JSC Mars-1A mixture, (b) the original JSC Mars-1A, (c) JSC Mars-1A after treatment at 800°C, (d) the NaCl–JSC Mars-1A mixture after treatment at 800°C, (e) the lecithin–NaCl–JSC Mars-1A mixture after treatment at 800°C and (f) sodalite (obtained from the RRUFF database).*

from the behaviour of neat lecithin, where long-chain polyphosphates formed. Whereas numerous phosphate minerals are known, there are only a few rare diphosphate minerals, at least on Earth (see e.g. Hudson Institute of Mineralogy, 2022b). Hence, diphosphate may be considered a potential biosignature. (ii) When a mixture of lecithin, NaCl and JSC Mars-1A was heated at 800°C, NaCl and the feldspar component of the Martian regolith simulant reacted to form the mineral sodalite. This finding is particularly interesting because it demonstrates the formation of a mineral under the influence of (the decomposition products of) biomolecules. Sodalite occurs on Earth in various geological settings, including volcanic ejecta (Hudson Institute of Mineralogy, 2022a). It is therefore probably of limited use as a (secondary) biosignature.

The thermal stability limit of the biomolecules studied here is about 240°C. This temperature may be compared with the surface temperatures that occur near lava flows. For example, on Kilauea volcano, Hawai'i, <175°C were measured at the upper surface of lava levees and 300–650°C at the inner walls

(Pinkerton *et al.*, 2002). Clearly, the biomolecules would not survive the high temperatures that occur in close proximity to lava flows. Nevertheless, some of their inorganic decomposition products such as graphite, metallic iron and diphosphate are relatively thermally stable and may serve as potential secondary biosignatures.

We would like to add a few cautionary notes regarding conclusions from studies of the thermal behaviour of chemical biosignatures:

(1) The biomolecules used are selected on the basis of terrestrial biochemistry. However, even when they are involved in basic biochemical functions in all known organisms, these molecules will not necessarily be present in extraterrestrial life. The same biochemical function can often be performed by different molecules. One-electron transfer, for example, is carried out by iron-porphyrin proteins, such as cytochrome *c*, but also by iron−sulphur and copper proteins (see e.g. Kaim *et al.*, 2013). It is quite conceivable that potential extraterrestrial biochemistries utilize completely different molecules – not only for one-electron transfer (see e.g. Bains, 2004).

(2) Heating experiments have several variables that may influence the outcome, especially when the thermal decomposition processes are complex. These variables include but are not limited to the heating rate, final temperature, annealing time and gas environment (static or flowing, composition). It is virtually impossible to study all combinations of factors that could be relevant. Therefore, the transferability of the results to hot natural environments is limited.

(3) In principle, organic molecules that are formed by thermal decomposition of biomolecules may themselves serve as biosignatures. However, if such molecules are found, for example, on Mars, it may be difficult or even impossible to prove their biogenicity because they could have resulted from prebiotic chemistry in the planet's past, or from meteoritic or cometary delivery. This problem often occurs with potential chemical biosignatures (Fox and Strasdeit, 2017).

References

Allen CC, Jager KM, Morris RV, Lindstrom DJ, Lindstrom MM and Lockwood JP (1998) Martian soil simulant available for scientific, educational study. *Eos* **79**, 405–412.

Bains W (2004) Many chemistries could be used to build living systems. *Astrobiology* **4**, 137–167.

Bardez I, Campayo L, Rigaud D, Chartier M and Calvet A (2008) Investigation of sodalites for conditioning halide salts (NaCl and NaI): comparison of two synthesis routes. In *Proceedings of ATALANTE 2008*, O4_19.

Barth A (2007) Infrared spectroscopy of proteins. *Biochimica et Biophysica Acta* **1767**, 1073–1101.

Barz A, Haase T, Meyer K and Stachel D (1996) Corrosion of crucible materials and their influence on structure of phosphate glasses. *Phosphorus Research Bulletin* **6**, 331–335.

Bertini I, Cavallaro G and Rosato A (2006) Cytochrome *c*: occurrence and functions. *Chemical Reviews* **106**, 90–115.

Bibring J-P, Hamm V, Pilorget C, Vago JL and the MicrOmega Team (2017) The MicrOmega investigation onboard ExoMars. *Astrobiology* **17**, 621–626.

Bohle DS, Dodd EL and Stephens PW (2012) Structure of malaria pigment and related propanoate-linked metalloporphyrin dimers. *Chemistry & Biodiversity* **9**, 1891–1902.

Bues W and Gehrke H-W (1957) Schwingungsspektren geschmolzener, glasiger und kristallisierter hochpolymerer Phosphate. *Zeitschrift für anorganische und allgemeine Chemie* **288**, 307–323.

Callot HJ and Ocampo R (2000) Geochemistry of porphyrins. In Kadish KM, Smith KM and Guilard R (eds), *The Porphyrin Handbook, Volume 1: Synthesis and Organic Chemistry*. San Diego: Academic Press, pp. 349–398.

Campos IB, Nantes IL, Rodrigues FA and Brochsztain S (2004) Photoinduced electron transfer in silica-supported self-assembled thin films containing a 1,4,5,8-naphthalenetetracarboxylic diimide and cytochrome *c*. *Journal of Materials Chemistry* **14**, 54–60.

Carr MH (2012) The fluvial history of Mars. *Philosophical Transactions of the Royal Society A* **370**, 2193–2215.

Castellini E, Malferrari D, Bernini F, Brigatti MF, Castro GR, Medici L, Mucci A and Borsari M (2017) Baseline studies of The Clay Minerals Society Source Clay montmorillonite STx-1b. *Clays and Clay Minerals* **65**, 220–233.

Cloutis EA, Mann P, Izawa MRM, Applin DM, Samson C, Kruzelecky R, Glotch TD, Mertzman SA, Mertzman KR, Haltigin TW and Fry C (2015) The Canadian space agency planetary analogue materials suite. *Planetary and Space Science* **119**, 155–172.

Corbridge DEC and Lowe EJ (1954) The infra-red spectra of some inorganic phosphorus compounds. *Journal of the Chemical Society*, 493–502.

Cornilsen BC and Condrate Sr RA (1978) The vibrational spectra of α-alkaline earth pyrophosphates. *Journal of Solid State Chemistry* **23**, 375–382.

Dalai P, Pleyer HL, Strasdeit H and Fox S (2017) The influence of mineral matrices on the thermal behavior of glycine. *Origins of Life and Evolution of Biospheres* **47**, 427–452.

Deacon GB and Phillips RJ (1980) Relationships between the carbon–oxygen stretching frequencies of carboxylato complexes and the type of carboxylate coordination. *Coordination Chemistry Reviews* **33**, 227–250.

Deer WA, Howie RA and Zussman J (2013) *An Introduction to the Rock-Forming Minerals*, 3rd Edn. London: The Mineralogical Society, pp. 340–344.

De Sanctis MC, Altieri F, Ammannito E, Biondi D, De Angelis S, Meini M, Mondello G, Novi S, Paolinetti R, Soldani M, Mugnuolo R, Pirrotta S, Vago JL and the Ma_MISS team (2017) Ma_MISS on ExoMars: mineralogical characterization of the Martian subsurface. *Astrobiology* **17**, 612–620.

Dinegar RH (1982) The 1978 scientific study of the Shroud of Turin. *Shroud Spectrum International* **1**, 2–12.

Dörr S, Schade U and Hellwig P (2008) Far infrared spectroscopy on hemoproteins: a model compound study from 1800–100 cm^{-1}. *Vibrational Spectroscopy* **47**, 59–65.

Doty KC, Muro CK and Lednev IK (2017) Predicting the time of the crime: bloodstain aging estimation for up to two years. *Forensic Chemistry* **5**, 1–7.

Downs RT and Hall-Wallace M (2003) The American Mineralogist crystal structure database. *American Mineralogist* **88**, 247–250.

Ehlmann BL and Edwards CS (2014) Mineralogy of the Martian surface. *Annual Review of Earth and Planetary Sciences* **42**, 291–315.

Eicher T, Hauptmann S and Speicher A (2012) *The Chemistry of Heterocycles*, 3rd Edn. Weinheim, Germany: Wiley-VCH, pp. 297–305 and 420–423.

Farley KA, Williford KH, Stack KM, Bhartia R, Chen A, de la Torre M, Hand K, Goreva Y, Herd CDK, Hueso R, Liu Y, Maki JN, Martinez G, Moeller RC, Nelessen A, Newman CE, Nunes D, Ponce A, Spanovich N, Willis PA, Beegle LW, Bell III JF, Brown AJ, Hamran S-E, Hurowitz JA, Maurice S, Paige DA, Rodriguez-Manfredi JA, Schulte M and Wiens RC (2020) Mars 2020 mission overview. *Space Science Reviews* **216**, 142.

Fitch WM (1976) The molecular evolution of cytochrome *c* in eukaryotes. *Journal of Molecular Evolution* **8**, 13–40.

Fox S and Strasdeit H (2013) A possible prebiotic origin on volcanic islands of oligopyrrole-type photopigments and electron transfer cofactors. *Astrobiology* **13**, 578–595.

Fox S and Strasdeit H (2017) Inhabited or uninhabited? Pitfalls in the interpretation of possible chemical signatures of extraterrestrial life. *Frontiers in Microbiology* **8**, 1622.

Fox S, Pleyer HL and Strasdeit H (2019) An automated apparatus for the simulation of prebiotic wet–dry cycles under strictly anaerobic conditions. *International Journal of Astrobiology* **18**, 60–72.

Goesmann F, Brinckerhoff WB, Raulin F, Goetz W, Danell RM, Getty SA, Siljeström S, Mißbach H, Steininger H, Arevalo Jr RD, Buch A, Freissinet C, Grubisic A, Meierhenrich UJ, Pinnick VT, Stalport F, Szopa C, Vago JL, Lindner R, Schulte MD, Brucato JR, Glavin DP, Grand N, Li X, van Amerom FHW and the MOMA Science Team (2017) The Mars Organic Molecule Analyzer (MOMA) instrument: characterization of organic material in Martian sediments. *Astrobiology* **17**, 655–685.

Greeley R and Spudis PD (1981) Volcanism on Mars. *Reviews of Geophysics and Space Physics* **19**, 13–41.

Greenwalt DE, Goreva YS, Siljeström SM, Rose T and Harbach RE (2013) Hemoglobin-derived porphyrins preserved in a Middle Eocene blood-engorged mosquito. *Proceedings of the National Academy of Sciences of the USA* **110**, 18496–18500.

Greenwood NN and Earnshaw A (1997) *Chemistry of the Elements*, 2nd Edn. Oxford, UK: Butterworth-Heinemann, pp. 526–531.

Hauber E, Brož P, Jagert F, Jodłowski P and Platz T (2011) Very recent and wide-spread basaltic volcanism on Mars. *Geophysical Research Letters* **38**, L10201.

Hudson Institute of Mineralogy (2022a) Sodalite: mineral information, data and localities. Available at https://www.mindat.org/min-3701.html (accessed 26 May 2022).

Hudson Institute of Mineralogy (2022b) Canaphite: mineral information, data and localities. Available at https://www.mindat.org/min-877.html (accessed 26 May 2022).

Jakosky BM and Phillips RJ (2001) Mars' volatile and climate history. *Nature* **412**, 237–244.

Jastrzębski W, Sitarz M, Rokita M and Bułat K (2011) Infrared spectroscopy of different phosphates structures. *Spectrochimica Acta Part A: Molecular and Biomolecular Spectroscopy* **79**, 722–727.

Kaduk JA, Wong-Ng W, Cook LP, Chakraborty B, Lapidus SH, Ribaud L and Brewer G (2016) Synchrotron X-ray investigation of α-chlorohemin, $C_{34}H_{32}ClFeN_4O_4$, an Fe-porphyrin. *Solid State Sciences* **53**, 63–70.

Kaim W, Schwederski B and Klein A (2013) *Bioinorganic Chemistry: Inorganic Elements in the Chemistry of Life*, 2nd Edn. Chichester: Wiley, pp. 117–130, 183–191.

Kaza N, Ojaghi A and Robles FE (2021) Hemoglobin quantification in red blood cells via dry mass mapping based on UV absorption. *Journal of Biomedical Optics* **26**, 086501.

Kite ES (2019) Geologic constraints on early Mars climate. *Space Science Reviews* **215**, 10.

Klöck W, Palme H and Tobschall HJ (1986) Trace elements in natural metallic iron from Disko Island, Greenland. *Contributions to Mineralogy and Petrology* **93**, 273–282.

Koenig DF (1965) The structure of α-chlorohemin. *Acta Crystallographica* **18**, 663–673.

Krasnopolsky VA (2011) Atmospheric chemistry on Venus, Earth, and Mars: main features and comparison. *Planetary and Space Science* **59**, 952–964.

Kudo S and Nakashima S (2020) Changes in IR band areas and band shifts during water adsorption to lecithin and ceramide. *Spectrochimica Acta Part A: Molecular and Biomolecular Spectroscopy* **228**, 117779.

Lafuente B, Downs RT, Yang H and Stone N (2015) The power of databases: the RRUFF project. In Armbruster T and Danisi RM (eds), *Highlights in Mineralogical Crystallography*. Berlin: De Gruyter, pp. 1–30.

Makreski P, Jovanovski G and Dimitrovska S (2005) Minerals from Macedonia: XIV. Identification of some sulfate minerals by vibrational (infrared and Raman) spectroscopy. *Vibrational Spectroscopy* **39**, 229–239.

Mandon L, Parkes Bowen A, Quantin-Nataf C, Bridges JC, Carter J, Pan L, Beck P, Dehouck E, Volat M, Thomas N, Cremonese G, Tornabene LL and Thollot P (2021) Morphological and spectral diversity of the clay-bearing unit at the ExoMars landing site Oxia Planum. *Astrobiology* **21**, 464–480.

McKay CP (2010) An origin of life on Mars. *Cold Spring Harbor Perspectives in Biology* **2**, a003509.

Mochidzuki K, Soutric F, Tadokoro K, Antal Jr MJ, Tóth M, Zelei B and Várhegyi G (2003) Electrical and physical properties of carbonized charcoals. *Industrial & Engineering Chemistry Research* **42**, 5140⍰⍰5151.

Nirmala R, Park H-M, Navamathavan R, Kang H-S, El-Newehy MH and Kim HY (2011) Lecithin blended polyamide-6 high aspect ratio nanofiber scaffolds via electrospinning for human osteoblast cell culture. *Materials Science and Engineering C* **31**, 486–493.

Parikh SJ, Kubicki JD, Jonsson CM, Jonsson CL, Hazen RM, Sverjensky DA and Sparks DL (2011) Evaluating glutamate and aspartate binding mechanisms to rutile (α-TiO$_2$) via ATR-FTIR spectroscopy and quantum chemical calculations. *Langmuir* **27**, 1778–1787.

Pasek MA (2020) Thermodynamics of prebiotic phosphorylation. *Chemical Reviews* **120**, 4690–4706.

Petrone P, Pucci P, Vergara A, Amoresano A, Birolo L, Pane F, Sirano F, Niola M, Buccelli C and Graziano V (2018) A hypothesis of sudden body fluid vaporization in the 79 AD victims of Vesuvius. *PLoS ONE* **13**, e0203210.

Pinkerton H, James M and Jones A (2002) Surface temperature measurements of active lava flows on Kilauea volcano, Hawai´i. *Journal of Volcanology and Geothermal Research* **113**, 159–176.

Pleyer HL, Moeller R, Fujimori A, Fox S and Strasdeit H (2022) Chemical, thermal, and radiation resistance of an iron porphyrin: a model study of biosignature stability. *Astrobiology* **22**, 776–799.

Popova AV and Hincha DK (2003) Intermolecular interactions in dry and rehydrated pure and mixed bilayers of phosphatidylcholine and digalactosyldiacylglycerol: a Fourier transform infrared spectroscopy study. *Biophysical Journal* **85**, 1682–1690.

Rao KJ, Sobha KC and Kumar S (2001) Infrared and Raman spectroscopic studies of glasses with NASICON-type chemistry. *Proceedings of the Indian Academy of Sciences (Chemical Sciences)* **113**, 497–514.

Rull F, Maurice S, Hutchinson I, Moral A, Perez C, Diaz C, Colombo M, Belenguer T, Lopez-Reyes G, Sansano A, Forni O, Parot Y, Striebig N, Woodward S, Howe C, Tarcea N, Rodriguez P, Seoane L, Santiago A, Rodriguez-Prieto JA, Medina J, Gallego P, Canchal R, Santamaría P, Ramos G, Vago JL and on behalf of the RLS Team (2017) The Raman Laser Spectrometer for the ExoMars rover mission to Mars. *Astrobiology* **17**, 627–654.

Russo C, Stanzione F, Tregrossi A and Ciajolo A (2014) Infrared spectroscopy of some carbon-based materials relevant in combustion: qualitative and quantitative analysis of hydrogen. *Carbon* **74**, 127–138.

Salama A, Neumann M, Günter C and Taubert A (2014) Ionic liquid-assisted formation of cellulose/calcium phosphate hybrid materials. *Beilstein Journal of Nanotechnology* **5**, 1553–1568.

Scholfield CR (1981) Composition of soybean lecithin. *Journal of the American Oil Chemists' Society* **58**, 889–892.

Schulze-Makuch D, Fairén AG and Davila AF (2008) The case for life on Mars. *International Journal of Astrobiology* **7**, 117–141.

Schweitzer MH, Marshall M, Carron K, Bohle DS, Busse SC, Arnold EV, Barnard D, Horner JR and Starkey JR (1997) Heme compounds in dinosaur trabecular bone. *Proceedings of the National Academy of Sciences of the USA* **94**, 6291–6296.

Shi SQ, Che W, Liang K, Xia C and Zhang D (2015) Phase transitions of carbon-encapsulated iron oxide nanoparticles during the carbonization of cellulose at various pyrolysis temperatures. *Journal of Analytical and Applied Pyrolysis* **115**, 1–6.

Smith BM and Franzen S (2002) Single-pass attenuated total reflection Fourier transform infrared spectroscopy for the analysis of proteins in H$_2$O solution. *Analytical Chemistry* **74**, 4076–4080.

Solomon SC, Aharonson O, Aurnou JM, Banerdt WB, Carr MH, Dombard AJ, Frey HV, Golombek MP, Hauck II SA, Head III JW, Jakosky BM, Johnson CL, McGovern PJ, Neumann GA, Phillips RJ, Smith DE and Zuber MT (2005) New perspectives on ancient Mars. *Science* **307**, 1214–1220.

Straasø T, Marom N, Solomonov I, Barfod LK, Burghammer M, Feidenhans'l R, Als-Nielsen J and Leiserowitz L (2014) The malaria pigment hemozoin comprises at most four different isomer units in two crystalline models: chiral as based on a biochemical hypothesis or centrosymmetric made of enantiomorphous sectors. *Crystal Growth & Design* **14**, 1543–1554.

Strasdeit H (2010) Chemical evolution and early Earth's and Mars' environmental conditions. *Palaeodiversity* **3** (Supplement), 107–116.

Strydom CA, Hudson-Lamb DL, Potgieter JH and Dagg E (1995) The thermal dehydration of synthetic gypsum. *Thermochimica Acta* **269/270**, 631–638.

Suo Z, Avci R, Schweitzer MH and Deliorman M (2007) Porphyrin as an ideal biomarker in the search for extraterrestrial life. *Astrobiology* **7**, 605–615.

Tantipolphan R, Rades T, McQuillan AJ and Medlicott NJ (2007) Adsorption of bovine serum albumin (BSA) onto lecithin studied by attenuated total reflectance Fourier transform infrared (ATR-FTIR) spectroscopy. *International Journal of Pharmaceutics* **337**, 40–47.

Umbreit J (2007) Methemoglobin – it's not just blue: a concise review. *American Journal of Hematology* **82**, 134–144.

Vago JL, Westall F and Pasteur Instrument Teams, Landing Site Selection Working Group and other contributors (2017) Habitability on early Mars and the search for biosignatures with the ExoMars rover. *Astrobiology* **17**, 471–510.

Van Meer G, Voelker DR and Feigenson GW (2008) Membrane lipids: where they are and how they behave. *Nature Reviews Molecular Cell Biology* **9**, 112–124.

Voigt JRC and Hamilton CW (2018) Investigating the volcanic versus aqueous origin of the surficial deposits in Eastern Elysium Planitia, Mars. *Icarus* **309**, 389–410.

Wang Q, Zhou Z, Chen D, Lin J, Ke F, Xu G and Sun S (2010) Study of pyrolyzed hemin/C as non-platinum cathodic catalyst for direct methanol fuel cells. *Science China Chemistry* **53**, 2057–2062.

Westall F and Cavalazzi B (2011) Biosignatures in rocks. In Reitner J and Thiel V (eds), *Encyclopedia of Geobiology*. Dordrecht: Springer, pp. 189–201.

Westall F, Foucher F, Bost N, Bertrand M, Loizeau D, Vago JL, Kminek G, Gaboyer F, Campbell KA, Bréhéret J-G, Gautret P and Cockell CS (2015) Biosignatures on Mars: what, where, and how? Implications for the search for Martian life. *Astrobiology* **15**, 998–1029.

Xiao L, Huang J, Christensen PR, Greeley R, Williams DA, Zhao J and He Q (2012) Ancient volcanism and its implication for thermal evolution of Mars. *Earth and Planetary Science Letters* **323–324**, 9–18.